

## Double-vertically-stacked Josephson junctions: Numerical and analytical analyses of a current-biased system in a magnetic field

S. R. Maglic, P. R. Auvil, Jr., and J. B. Ketterson

*Department of Physics and Astronomy, Northwestern University, Evanston, Illinois 60208*

(Received 14 July 1998)

We examine the solutions of the nonlinear equations governing the behavior of a current-biased, double-vertically-stacked, Josephson junction. Both inline and overlap biasing current geometries are considered. The solution space is investigated analytically and using numerical techniques. We characterize the types of solutions expected analytically for zero current and find good approximations for large magnetic fields. We study this space and its stability as a function of magnetic field and applied bias current. Selective results are presented that characterize the general behavior of the solution space. [S0163-1829(99)04101-6]

### I. INTRODUCTION

The motivation for this work comes from recent experimental measurements of  $I$  versus  $H$  in vertically-stacked Josephson junctions. These measurements have been made by our own group<sup>1</sup> as well as others.<sup>2,3</sup> Also relevant is work done on high-temperature and superconducting materials.<sup>4</sup> The general equations governing the behavior of stacked junctions were presented by Sakai, Bodin, and Pedersen.<sup>5</sup> Examples of dynamic solutions were given in Ref. 5 and also by Kleiner *et al.*<sup>4</sup>

In this paper we look, in somewhat more detail than Refs. 4 and 5, at the double-junction case. We map out the complete solution space for the static junction in a magnetic field and at nonzero current. We consider both the inline and the overlap current biasing geometries. Behavior of the static solutions at nonzero current is analyzed. Plots similar to those for a single junction are presented (Refs. 6–10). We evaluate the time-dependent stability of each solution and discuss the various time-dependent modes of oscillation of the stable solutions.

We characterize the types of solutions that are expected by using a simple analytic model for the static solutions at zero bias current. This yields an accurate analytic approximation for large magnetic fields. For smaller magnetic fields we give numerical examples of the solution space. Enough detail is presented to reveal the structure of the solution space and the stability of the various solutions.

In Sec. II, we review the basic coupled sine-Gordon-like equations which govern the behavior of the static junction in a magnetic field. Both the inline and the overlap current biasing geometries are considered. Time-dependent terms are added so that a stability analysis of the solutions can be undertaken. In Sec. III, we derive a simple analytic model for the zero current static solutions. These approximate solutions are valid for large magnetic fields. However, they also serve to delineate the general solution types for all magnetic fields. In Sec. IV we present numerical solutions for the static junction with nonzero magnetic field and nonzero bias current. In Sec. V we include time-dependent terms in our equations and investigate the stability of the static solutions to small perturbations. For fixed magnetic field, the stability is evalu-

ated as the bias current is increased. The oscillation spectra of the stable solutions are discussed. Our conclusions are summarized in Sec. VI.

### II. THE BASIC EQUATIONS

We consider a one-dimensional model of a double-vertically-stacked Josephson junction of length  $L$  and denote the phase differences across the two junctions by  $\varphi_1(x)$  and  $\varphi_2(x)$ , where  $-L/2 \leq x \leq L/2$ . The inline and overlap geometries are depicted in Fig. 1, cases (a) and (b), respectively. A uniform magnetic field  $H$  is applied in the  $y$  direction. The current  $J$  flows in the  $x$  and  $y$  directions, respectively, in the two cases. We will always consider  $H \geq 0$  and  $J \geq 0$ . It is straightforward to see that this maps out the entire physical solution space. We assume that the junction is symmetric with insulating layers of thickness  $d$ . The central superconducting layer has thickness  $s$ , and we assume that the two outer superconducting layers are much thicker than the London penetration depth,  $\lambda_L$ . The effective thickness of each junction is  $d_{\text{eff}} = d + \lambda_L [1 + \coth(s/\lambda_L)]$ . The width of the junction is  $W$  and the Josephson currents are given by  $J_1(x) = J_c \sin(\varphi_1(x))$  and  $J_2(x) = J_c \sin(\varphi_2(x))$ .

The characteristic screening length for magnetic-field penetration into the junction is the Josephson depth  $\lambda_J$ , where  $(\lambda_J)^2 = \Phi / (2\pi\mu_0 d_{\text{eff}} J_c)$ , and  $\Phi = h/(2e)$  is the

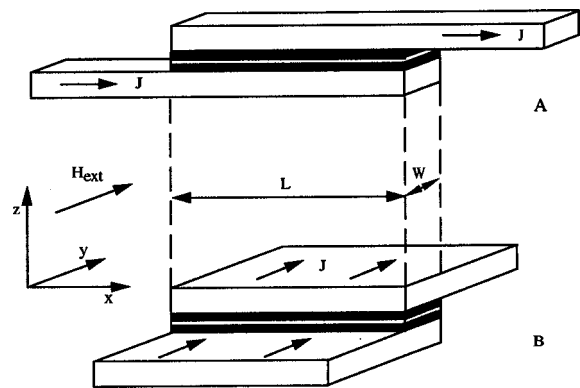


FIG. 1. Schematic of the inline (A) and overlap (B) geometries. The length and width of the junctions are  $L$  and  $W$ , respectively.

magnetic-flux quantum. We introduce the dimensionless length,  $\bar{x} = x/\lambda_J$ , current,  $R = J/J_c = JW_L/J_cWL = I/I_c$ , and magnetic field,  $h = (2\pi d_{\text{eff}}\lambda_J/\Phi)H$ . General equations for multilayer junctions in both current biasing schemes have been derived by Sakai, Bodin, and Pedersen.<sup>5</sup> For a double junction these equations become

$$d^2\varphi_1(\bar{x})/d\bar{x}^2 = \sin(\varphi_1(\bar{x})) + G \sin(\varphi_2(\bar{x})) - (1+G)R_0 \quad (1a)$$

and

$$d^2\varphi_2(\bar{x})/d\bar{x}^2 = \sin(\varphi_2(\bar{x})) + G \sin(\varphi_1(\bar{x})) - (1+G)R_0 \quad (1b)$$

with boundary conditions

$$d\varphi_1(\pm\bar{L}/2)/d\bar{x} = (1+G)(h \pm R_i\bar{L}/2) \quad (2a)$$

and

$$d\varphi_2(\pm\bar{L}/2)/d\bar{x} = (1+G)(h \pm R_i\bar{L}/2), \quad (2a)$$

where  $G = -\lambda_L/[d_{\text{eff}} \sinh(s/\lambda_L)]$  is the intralayer coupling parameter. As expected, for  $s/\lambda_L \gg 1$ ,  $d_{\text{eff}} \cong d + 2\lambda_L$  and  $G \cong 0$ . In what follows, in order to restrict the number of parameters, we will use  $G = -0.75$ . This value is typical of the coupling used in Ref. 1.

Note that  $R_i$  (the relative current in the inline case) and  $R_0$  (the relative current in the overlap case) are never both non-zero. Solutions exist only for  $R_i$  and/or  $R_0 \leq 1$ . In the case where  $R_i$ ,  $R_0$ , and  $G$  are all equal to zero, Eqs. (1a), (1b), and (2a), (2b) can be solved analytically in terms of elliptic integrals (see Ref. 6). However, the solution space is so large that numerical solutions are easier to use than the exact analytic results.

To investigate the stability of the static solutions, we add a wave-like coupling and a damping term to Eqs. (1a), (1b). On the right-hand side of Eqs. (1a), (1b) we add the extra terms

$$d^2\varphi_1(\bar{x}, \bar{t})/d\bar{t}^2 + \beta d\varphi_1(\bar{x}, \bar{t})/d\bar{t} \quad (3a)$$

and

$$d^2\varphi_2(\bar{x}, \bar{t})/d\bar{t}^2 + \beta d\varphi_2(\bar{x}, \bar{t})/d\bar{t} \quad (3b)$$

to the two equations, respectively, where  $\bar{t} = (2\pi J_c/\Phi C)^{1/2}t$  and  $\beta = (\Phi/2\pi J_c C)^{1/2}g$ ;  $C$  and  $g$  are the capacitance and the conductance per unit area of the junction, respectively.<sup>5</sup>

### III. APPROXIMATE STATIC SOLUTIONS WITH ZERO CURRENT

In order to anticipate the types of solutions that we will find by numerical methods, it is useful to introduce approximate solutions to Eqs. (1a), (1b) and (2a), (2b) in the zero current case. As we shall see, these solutions are only valid for  $h \gg 1$ , but solutions of a similar type persist for all values of the magnetic field.

To find an approximate solution to Eqs. (1a), (1b), we iterate the zeroth-order solutions in which the terms on the right-hand sides are neglected. Thus, we expect  $\varphi_1(\bar{x}) \cong a_1$

+  $b_1\bar{x}$  and  $\varphi_2(\bar{x}) \cong a_2 + b_2\bar{x}$ . Using this as input, our next approximation becomes

$$\begin{aligned} \varphi_1(\bar{x}) \cong & a_1 + b_1\bar{x} - [\sin(a_1 + b_1\bar{x})]/b_1^2 \\ & - G[\sin(a_2 + b_2\bar{x})]/b_2^2 \end{aligned} \quad (4a)$$

and

$$\begin{aligned} \varphi_2(\bar{x}) \cong & a_2 + b_2\bar{x} - [\sin(a_2 + b_2\bar{x})]/b_2^2 \\ & - G[\sin(a_1 + b_1\bar{x})]/b_1^2. \end{aligned} \quad (4b)$$

For our purposes this is sufficient. Our boundary conditions, Eqs. (2a), (2b), become

$$b_1 - [\cos(a_1 - b_1\bar{L}/2)]/b_1 - G[\cos(a_2 - b_2\bar{L}/2)]/b_2 = h, \quad (5a)$$

$$b_1 - [\cos(a_1 + b_1\bar{L}/2)]/b_1 - G[\cos(a_2 + b_2\bar{L}/2)]/b_2 = h, \quad (5b)$$

$$b_2 - [\cos(a_2 - b_2\bar{L}/2)]/b_2 - G[\cos(a_1 - b_1\bar{L}/2)]/b_1 = h, \quad (5c)$$

and

$$b_2 - [\cos(a_2 + b_2\bar{L}/2)]/b_2 - G[\cos(a_1 + b_1\bar{L}/2)]/b_1 = h. \quad (5d)$$

Expanding the cosine terms in Eqs. (5a)–(5d), we find four conditions

$$\sin(a_1)\sin(b_1\bar{L}/2) = 0, \quad (6a)$$

$$\sin(a_2)\sin(b_2\bar{L}/2) = 0, \quad (6b)$$

$$\begin{aligned} b_1 - \cos(a_1)\cos(b_1\bar{L}/2)/b_1 \\ - G \cos(a_2)\cos(b_2\bar{L}/2)/b_2 = h \end{aligned} \quad (7a)$$

and

$$\begin{aligned} b_2 = [\cos(a_2)\cos(b_2\bar{L}/2)]/b_2 \\ - G \cos(a_1)\cos(b_1\bar{L}/2)/b_1 = h. \end{aligned} \quad (7b)$$

Note that the boundary conditions, Eqs. (5), involve the constant  $G$  where the latter was eliminated in Eqs. (6a), (6b) by taking appropriate linear combinations. From Eqs. (7a), (7b), and our approximate solutions Eqs. (4a), (4b) it follows that  $b_1$  and  $b_2$  are of order  $h$  for large  $h$ . This is the region where we expect our approximate solutions to be valid, which is confirmed by our numerical calculations. However, these approximate solutions are also valuable for classifying the numerical solutions.

Using Eqs. (6a), (6b) the solutions are of three types:

$$(1) \text{ Both } \sin(b_1\bar{L}/2) = 0 \text{ and } \sin(b_2\bar{L}/2) = 0,$$

$$(2) \text{ Both } \sin(a_1) = 0 \text{ and } \sin(a_2) = 0,$$

and

$$(3) \sin(a_1) = 0 \text{ and } \sin(b_2\bar{L}/2) = 0 \text{ or visa versa.}$$

Solutions of type (1) are referred to as ‘‘fluxon’’ solutions. To see why this is true, we need to recall that within each junction, the magnetic field is related to  $\varphi_{1,2}(x)$  by

$$H_{1,2}(x) = (\Phi/2\pi d_{\text{eff}}) d\varphi_{1,2}(x)/dx. \quad (8)$$

Thus, the effective flux in a junction is

$$\phi_{1,2} = d_{\text{eff}} \int H_{1,2}(x) dx = (\Phi/2\pi) [\varphi_{1,2}(\bar{L}/2) - \varphi_{1,2}(-\bar{L}/2)]. \quad (9)$$

When  $b_1\bar{L}/2 = m_1\pi$  and  $b_2\bar{L}/2 = m_2\pi$ , Eqs. (4a), (4b) yield  $\varphi_1(\bar{L}/2) - \varphi_1(-\bar{L}/2) = b_1\bar{L} = 2m_1\pi$  and  $\varphi_2(\bar{L}/2) - \varphi_2(-\bar{L}/2) = b_2\bar{L} = 2m_2\pi$ . Therefore,  $\phi_1 = m_1\Phi$  and  $\phi_2 = m_2\Phi$ ; i.e., we have  $m_1$  units of the magnetic-flux quantum in the upper junction and  $m_2$  units in the lower junction.

Referring to Eqs. (7) we see that because the cosine function is restricted to lie between the plus and minus one, type (1) solutions will exist only for a certain range of  $h$  values, if at all. When each of the junctions has  $m$  fluxons, this condition becomes

$$b - (1+G)/b \leq h \leq b + (1+G)/b \quad (10)$$

with  $b = 2m\pi/\bar{L}$ . When the two junctions contain  $m_1$  and  $m_2$  fluxons, respectively, there may or may not be a range of  $h$  where Eqs. (7) can both be satisfied. However, if there is one solution, then there are many. First, there is an essentially identical solution with  $m_1$  fluxons in the bottom junction and  $m_2$  fluxons in the top junction. Second, Eqs. (7) determine only the cosine of  $a_1$  and  $a_2$  so that solutions exist for the combinations,  $\pm a_1$  and  $\pm a_2$ . Note that if both angles change sign, this produces a solution with the magnetic field reflected about  $x=0$  in both junctions, i.e.,  $H(x) \rightarrow H(-x)$ . For example, we find numerically that when  $\bar{L}=17$ ,  $h=3$ , and  $G=-0.75$ , there are solutions with eight fluxons in each junction and solutions with seven fluxons in one junction and nine fluxons in the other.

Type (2) solutions are characterized by  $\varphi_1(0)=0$  or  $\pi$  and  $\varphi_2(0)=0$  or  $\pi$ . Type (3) solutions are a bit more difficult to identify. However, with some algebra it can be shown that if  $b_1\bar{L}/2 = n_1\pi$  and  $a_2 = m_2\pi$ , then for even values of  $n_1$ ,  $\varphi_2(0) = [\varphi_2(\bar{L}/2) + \varphi_2(-\bar{L}/2)]/2$  and for odd values of  $n_1$ ,  $\varphi_2(0) = -[\varphi_2(\bar{L}/2) + \varphi_2(-\bar{L}/2)]/2 + 2m_2\pi$ . The same equations hold with the subscripts reversed.

Our numerical calculations at zero bias current show that all solutions fall into one of the three above types. For example when  $\bar{L}=3$  and  $h=4.5$  with  $G=-0.75$ , we find eight solutions: four of type (2) and four of type (3). When  $\bar{L}=3$  and  $h=6.3$  with  $G=-0.75$ , we find eight solutions: four of type (1) with three fluxons in each junction and four of type (2). Further study shows that for large enough values of  $h$  where our approximate solutions are valid, solutions of type (2) exist for all values of  $h$ , whereas type (1) and type (3) solutions only exist for certain ranges of  $h$ . For example, for  $\bar{L}=3$  type (1) solutions with two fluxons exist only for  $4.12 \leq h \leq 4.24$  and type (3) solutions with  $N1=2$  exist only for  $3.75 \leq h \leq 4.54$ .

In a previous paper, Ref. 10, we studied the solutions to the single-junction problem. These solutions, suitably scaled,

form a subset of the solutions to the double junction. If we look for solutions of Eqs. (4) with equal phase in each junction,  $\varphi_1(\bar{x}) = \varphi_2(\bar{x})$ , then a solution in a single junction of length  $\bar{L}_s = (1+G)^{1/2}\bar{L}$  and reduced magnetic field  $h_s = h/(1+G)^{1/2}$  satisfies the double-junction equations. For example, a single junction of length  $\bar{L}_s = 1.5$  and  $h_s = 9$  has solutions that can be used to find equal phase solutions for a double junction of length  $\bar{L} = 3$  and  $h = 4.5$  when  $G = -0.75$ . As was shown in Ref. 10, a single junction with large  $h_s$  has two types of solutions. For certain ranges of  $h_s$ , fluxon type solutions exist. For all values of  $h_s$ , two solutions exist: one with  $\varphi(0)=0$  and one with  $\varphi(0)=\pi$ . For this value,  $h_s=9$ , only the two nonfluxon solutions exist. When translated into solutions for the double junction they produce two of the eight solutions noted in the previous paragraph. The remaining six solutions for this case have nonequal values of their phases in the two junctions. Note that in some sense there are really only three distinct extra solutions because each solution with nonequal phases produces another solution with the phases in the junctions interchanged.

Solutions can also be identified by their symmetry. By examining Eqs. (1) it is easy to see that we can always generate a second solution set by the symmetry operation,  $\tilde{\varphi}_1(\bar{x}) = \pm \varphi_1(-\bar{x})$  and  $\tilde{\varphi}_2(\bar{x}) = \pm \varphi_2(-\bar{x})$ . Fluxon solutions always come in pairs and this symmetry operation transforms between them. Solutions of type (2) transform themselves into modulo  $2\pi$  so that  $\tilde{\varphi}_1(\bar{x}) = \varphi_1(\bar{x}) - 2m_1\pi$  and  $\tilde{\varphi}_2(\bar{x}) = \varphi_2(\bar{x}) - 2m_2\pi$ . The symmetry operation generates a second type (3) solution, but it has no distinguishing symmetry characteristics.

#### IV. NUMERICAL STATIC SOLUTIONS FOR ZERO AND NONZERO CURRENT

In this section we treat in detail the case of an overlap junction of length  $\bar{L}=3$  with both nonzero magnetic field and bias current. As previously mentioned, we always choose  $G=-0.75$  in our examples. Solutions of Eqs. (1) and the four boundary conditions contained in Eqs. (2) are obtained computationally with an adapted ‘‘RshootingS’’ approach. To specify a unique solution, the two second-order differential equations require four boundary conditions. With  $d\varphi_{1,2}(-\bar{L}/2)/d\bar{x}$  fixed by Eqs. (2), we are therefore required to vary the free parameters  $\varphi_{1,2}(-\bar{L}/2)$  until  $d\varphi_{1,2}(+\bar{L}/2)/d\bar{x}$  satisfy the boundary conditions, Eqs. (2). However, because the system is invariant under the transformation  $\varphi_1(\bar{x}) = \varphi_1(\bar{x}) + 2\pi$  [and similarly for  $\varphi_2(\bar{x})$ ], we are able to span the entire solution space by varying  $\varphi_1(\bar{x})$  and  $\varphi_2(\bar{x})$  over a range of  $2\pi$ . The parameter space is broken up into a lattice and the Cauchy problem is solved by fourth-order Runge-Kutta integration. Each time the integration is performed

$$d1 = d\varphi_1(+\bar{L}/2)d\bar{x} - d\varphi_1(-\bar{L}/2)d\bar{x} - (1+G)R_i\bar{L} \quad (11a)$$

and

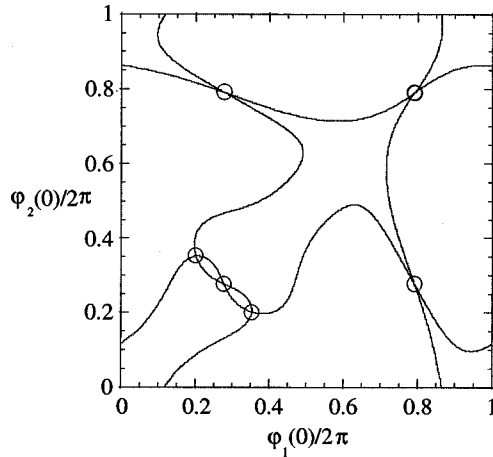


FIG. 2. The phase space for numerical solutions for  $\bar{L}=3$ ,  $h=3$ ,  $R=0$ , and  $G=-0.75$  with a lattice spacing of  $2\pi/500$  on a side. A data point is plotted where either  $d1$  or  $d2$  is zero. The dense series of points appears as a solid line. The open circles indicate a solution point.

$$d2 = d\phi_2(+\bar{L}/2)d\bar{x} - d\phi_2(-\bar{L}/2)d\bar{x} - (1+G)R_0\bar{L} \quad (11b)$$

are monitored and compared with neighboring lattice sites. Using first-order interpolation it is determined if and where both  $d1$  and  $d2$  vanish. The solutions can be obtained quite effectively provided that the lattice spacing is chosen sufficiently small. Figure 2 shows the parameter space for  $h=3$  and  $R=0$  with a square lattice of  $2\pi/500$  on a side. On the plot a data point appears when either  $d1$  or  $d2$  goes to zero. A dense series of points appears on the plot as a line. Large open circles indicate where the interpolation algorithm has successfully found  $d1=d2=0$ . Plots of this type are made to verify that the algorithm is working properly and to distinguish distinct solutions. The large open circles explicitly show the six solutions for  $\bar{L}=3$ ,  $h=3$  and  $R=0$ . Also, the symmetry intrinsic to the system appears in the solution space.

Figures 3(A)–3(D) show the magnetic-field variation within the junction for the different solutions. Four sets of plots are shown because the antisymmetric solutions are identical if one interchanges the boundary conditions in the two junctions. Two solutions, Figs. 3(A) and 3(B), have equal magnetic fields in the two junctions. As discussed in Sec. III, these two solutions correspond to single-junction solutions with  $\bar{L}_s=1.5$  and  $h_s=6$ . We note that solutions are available in the double junction where the distribution of the magnetic field in one junction is maximum where the magnetic field is minimum in the adjacent one. We also note that this pattern corresponds to the magnetic-flux quanta arranged in a triangular array. Stability of this flux arrangement was discussed by Kivshar and Soboleva.<sup>11</sup> In terms of our classification of solutions in Sec. III, all six of these solutions are of type (2).

Figure 4 presents the current versus magnetic-field characteristic of a double overlap junction of length  $\bar{L}=3$  and a coupling constant,  $G=-0.75$ . The solid lines represent the critical current for each of the related solutions. For the sake

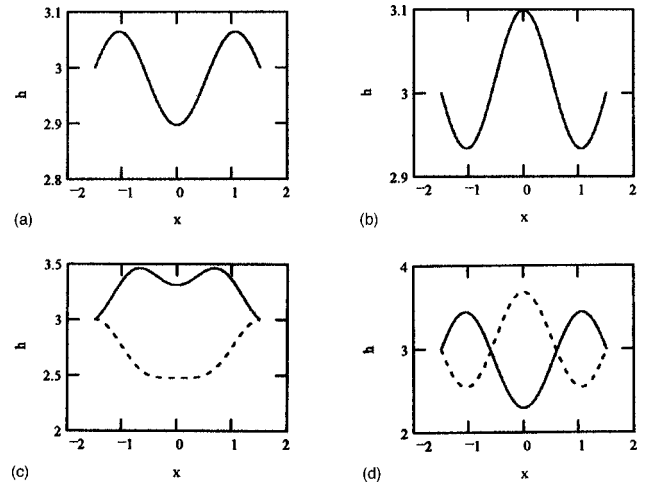


FIG. 3. The six solutions [(A), (B), (C), and (D)] for  $\bar{L}=3$ ,  $h=3$ ,  $R=0$ , and  $G=-0.75$ . (C) and (D) represent two solutions each with the magnetic fields  $h$  in the junctions interchanged.

of comparison, characteristics of the single layer junction (indicated with dashed lines) are superimposed. As  $R_0$  increases, solutions cease to exist in pairs. Therefore, under each boundary lobe there are two solutions. At  $h=3$  there are three lobes corresponding to the six  $R_0=0$  solutions described above and shown in Fig. 3. Similarly at other values of the magnetic field at  $R_0=0$ , there exist: six solutions at  $h=0$ , four solutions at  $h=1$ , eight solutions at  $h=2$ , six solutions at  $h=3$ , eight solutions at  $h=4$ , etc. For example, in terms of our classification of solutions in Sec. III, at  $h=2$ : two solutions are of type (1) with one fluxon, four solutions are of type (2), and two solutions are of type (3). At  $h=4$ : four solutions are of type (2) and four solutions are of type (3).

## V. TIME-DEPENDENT STABILITY

In order to access whether the preceding static solutions would be found in a real doubly-stacked, Josephson junction we need to study their stability. To do this we add the time-dependent terms of Eqs. (3) to Eqs. (1). Two approaches are possible. First, we could simply integrate the resulting equation starting at  $t=0$  with one of our static solutions (slightly perturbed). However, here we consider an alternative pertur-

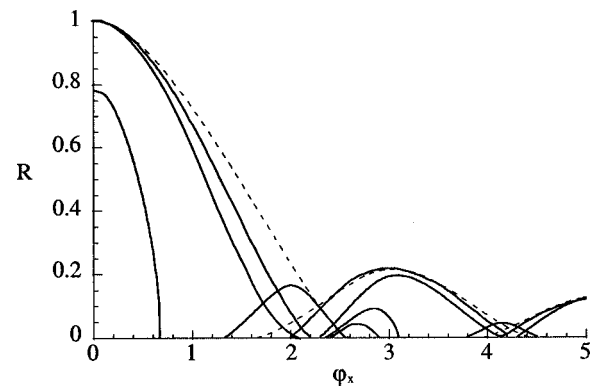


FIG. 4. Envelope of maximum bias current values for an overlap junction with  $\bar{L}=3$ ,  $h=3$ , and  $G=-0.75$ .

bative approach, which we showed in Ref. 10 produces satisfactory results for the single junction.

Let  $\varphi_{1,2}(\bar{x})$  be one of our static solution sets and consider  $\varphi_{1,2}(\bar{x}, \bar{t}) = \varphi_{1,2}(\bar{x}) + \delta_{1,2}(\bar{x}, \bar{t})$  for small  $\delta_{1,2}(\bar{x}, \bar{t})$ . This yields approximate equations of motion which are the same in both the inline and the overlap cases

$$d^2 \delta_1(\bar{x}, \bar{t})/d\bar{t}^2 + \beta d \delta_1(\bar{x}, \bar{t})/d\bar{t} = d^2 \delta_1(\bar{x}, \bar{t})/d\bar{x}^2 - \cos(\varphi_1(\bar{x})) \delta_1(\bar{x}, \bar{t}) - G \cos(\varphi_2(\bar{x})) \delta_2(\bar{x}, \bar{t}), \quad (12a)$$

$$d^2 \delta_2(\bar{x}, \bar{t})/d\bar{t}^2 + \beta d \delta_2(\bar{x}, \bar{t})/d\bar{t} = d^2 \delta_2(\bar{x}, \bar{t})/d\bar{x}^2 - \cos(\varphi_2(\bar{x})) \delta_2(\bar{x}, \bar{t}) - G \cos(\varphi_1(\bar{x})) \delta_1(\bar{x}, \bar{t}), \quad (12b)$$

where  $d \delta_{1,2}(\pm \bar{L}/2, \bar{t})/d\bar{x} = 0$ . Note we have a linear set of equations for  $\delta_{1,2}(\bar{x}, \bar{t})$ . We now look for solutions of the type  $\delta_{1,2}(\bar{x}, \bar{t}) = \delta_{1,2}(\bar{x}) e^{\omega \bar{t}}$  which yields

$$d^2 \delta_1(\bar{x})/d\bar{x}^2 - \cos(\varphi_1(\bar{x})) \delta_1(\bar{x}) - G \cos(\varphi_2(\bar{x})) \delta_2(\bar{x}) = \varepsilon \delta_1(\bar{x}), \quad (13a)$$

$$d^2 \delta_2(\bar{x})/d\bar{x}^2 - \cos(\varphi_2(\bar{x})) \delta_2(\bar{x}) - G \cos(\varphi_1(\bar{x})) \delta_1(\bar{x}) = \varepsilon \delta_2(\bar{x}), \quad (13b)$$

where  $d \delta_{1,2}(\pm \bar{L}/2)/d\bar{x} = 0$  and  $\varepsilon = \omega^2 + \beta \omega$ . Inverting this equation, we find two solutions,  $\omega_{\pm} = -\beta/2 \pm [(\beta/2)^2 + \varepsilon]^{1/2}$ . Thus, if a solution to Eqs. (13) has  $\varepsilon > 0$ , we also have  $\omega_+ > 0$  and the solution is unstable.

To study the properties of these solutions, it is convenient to introduce a matrix notation. We define

$$\delta(\bar{x}) = \begin{pmatrix} \delta_1(\bar{x}) \\ \delta_2(\bar{x}) \end{pmatrix} \quad (14)$$

and

$$H(\bar{x}) = \begin{pmatrix} \cos(\varphi_1(\bar{x})) & G \cos(\varphi_2(\bar{x})) \\ G \cos(\varphi_1(\bar{x})) & \cos(\varphi_2(\bar{x})) \end{pmatrix} \quad (15)$$

so that Eqs. (13) become

$$d^2 \delta(\bar{x})/d\bar{x}^2 - H(\bar{x}) \delta(\bar{x}) = \varepsilon \delta(\bar{x}). \quad (16)$$

To diagonalize  $H(\bar{x})$  we multiply Eq. (16) by the matrix

$$D = \begin{pmatrix} 1 & -G \\ -G & 1 \end{pmatrix}, \quad (17)$$

which yields

$$DH(\bar{x}) = \bar{H}(\bar{x}) = \begin{pmatrix} (1-G^2)\cos(\varphi_1(\bar{x})) & 0 \\ 0 & (1-G^2)\cos(\varphi_2(\bar{x})) \end{pmatrix}. \quad (18)$$

The equation for  $\delta(\bar{x})$  now becomes

$$d^2(D\delta(\bar{x}))/d\bar{x}^2 - \bar{H}(\bar{x})\delta(\bar{x}) = \varepsilon(D\delta(\bar{x})). \quad (19)$$

In this form, using the usual techniques, we can show that the eigenvalues  $\varepsilon$  are real and the solutions form an orthogonal set when convoluted with the matrix  $D$ . We have verified this with our numerical solutions. Numerically, we find that the fluxon-type solutions are degenerate (i.e., have the same  $\varepsilon$  value) at zero current, but all solutions are nondegenerate for nonzero current. To evaluate the stability of a given static solution, we look for the solution,  $\delta(\bar{x})$ , with the maximum value of  $\varepsilon$ . If that value is greater than zero, the solution is unstable. Numerically we find that solutions which are unstable at zero current do not become stable at nonzero current.

One might hope that the solutions which are stable at  $R = 0$  would be the ones that continue to exist for the highest values of  $R$ . Unfortunately, that is not the case. For example, referring to Fig. 4, at  $h = 2.4$  we see that some solutions persist to  $R_{\max} = 0.125$ . However, our numerical calculations show that the two solutions stable at  $R = 0$  cease to exist at  $R_{\max} = 0.05$ . Similarly, at  $h = 3$  and at  $h = 4.5$  we find that the solutions which are stable at  $R = 0$  are not the ones that persist to the highest  $R_{\max}$  values. These results for the double junction are not too surprising since we found similar results for a single junction in Ref. 10. In that paper we also looked at possible energy functionals which might be used to predict stability and the persistence of high current solutions. Extrema of these energy functionals did not yield predictions consistent with the stability analysis.

## VI. CONCLUSIONS

We have investigated in some detail the solutions of the equations for a Josephson junction in a magnetic field with nonzero current in both the inline and the overlap geometries. We found a useful approximation that yields a satisfying classification of the solution types. This same approximation gives an accurate approximation to our numerical solutions for large magnetic fields. For smaller fields we have mapped the solution space numerically. For the nonzero current we have mapped the maximum current envelope for each solution. Not all of the static solutions are stable. We have calculated the evolution of the solutions that are stable at zero current. Unfortunately, the solutions which appear to be the most stable at zero current, are not always the ones that persist to the highest current values. Likewise, in an attempt to predict this dependence using an energy criteria, we again found that the solutions with the lowest energy at zero current were not always the ones that persisted to the highest current values.

## ACKNOWLEDGMENT

The work was supported by the Northwestern Materials Research Center under NSF Grant No. OMR-91-20521.

- <sup>1</sup>S. N. Song, P. R. Auvil, M. P. Ulmer, and J. B. Ketterson, Phys. Rev. B **53**, R6018 (1996).
- <sup>2</sup>I. P. Nevirkovets, J. E. Evetts, and M. G. Blamire, Phys. Lett. A **187**, 119 (1994).
- <sup>3</sup>I. P. Nevirkovets, H. Kohlstedt, G. Hallmanns, and C. Hieden, Supercond. Sci. Technol. **6**, 146 (1993).
- <sup>4</sup>R. Kleiner, P. Muller, H. Kohlstedt, N. F. Pedersen, and S. Sakai, Phys. Rev. B **50**, 3942 (1994).
- <sup>5</sup>S. Sakai, P. Bodin, and N. F. Pedersen, J. Appl. Phys. **73**, 2411 (1993).
- <sup>6</sup>C. S. Owen and D. J. Scalapino, Phys. Rev. **164**, 538 (1967).
- <sup>7</sup>S. Pagano, B. Ruggiero, and E. Sarnelli, Phys. Rev. B **43**, 5364 (1991).
- <sup>8</sup>G. F. Zharkov and S. A. Vasenko, Sov. Phys. JETP **47**, 350 (1978).
- <sup>9</sup>S. A. Vasenko and G. F. Zharkov, Sov. Phys. JETP **48**, 89 (1978).
- <sup>10</sup>P. R. Auvil, S. R. Maglic, and J. B. Ketterson, J. Low Temp. Phys. (to be published).
- <sup>11</sup>Y. S. Kivshar and T. K. Soboleva, Phys. Rev. B **42**, 2655 (1990).